# Comparison of 2D and 3D PET for Cerebral FDG in Human Subjects

TR Oakes[1], JE Holden[2,3], RW Pyzalski[3], AD Roberts[1,4], WD Brown[3,2], RJ Nickles[2], RJ Davidson[1,4]

University of Wisconsin-Madison, Depts. of Psychology[1], Medical Physics[2], Radiology[3], Psychiatry[4]
Rm. 371, 1202 West Johnson St., Madison, WI 53706 U.S.A.

## *Abstract*

We compared 12 pairs of cerebral [$^{18}$F]-fluoro-deoxyglucose (FDG) 2D/3D image sets from a GE/Advance PET scanner, incorporating the actual corrections used on human subjects. Differences in resolution consistent with other published values [1-5] were found. There is a significant difference in axial resolution between 2D and 3D, and we focused on this as it is a scanner feature that cannot be readily changed. Previously published values for spatial axial resolution in 2D [1] and 3D [2] modes were used to model the differential axial smoothing at each image voxel. This model was applied to the 2D FDG images, and the resulting smoothed data indicate the published differences in axial resolution between 2D and 3D modes can account for 30-40% of the differences between these image sets.

We then investigated the effect this difference might have on analysis typically performed on human FDG data. A phantom containing spherical hot- and cool-spots in a warm background to mimic a typical human cerebral FDG PET scan was scanned for a variety of time durations (30, 15, 5, 1 min). Only for the 1-minute frame (total counts 2D:6M, 3D:30M) is there an advantage to using 3D mode; for the longer frames which are more typical of a human FDG protocol, the reliability for extracting regions-of-interest is the same for either mode while 2D mode shows better quantitative accuracy.

## I. Introduction

The GE/Advance PET scanner has been nicely characterized in 2D mode [1] and 3D mode [2-4] using a variety of phantoms. For this and other scanners there is a thriving body of published literature examining the differences between 2D and 3D modes [5-9], and in optimizing 3D mode parameters for various situations [10-19]. Generally speaking, 3D PET shows an increase in sensitivity by a factor of ~6 [9, 20, 21] that can yield a gain in the signal-to-noise ratio (SNR) and a consequent improvement in image quality.

However, potentially deleterious factors, such as an increase in the fraction of scattered photons by a factor of 2-4 [10, 19-21], can offset or even negate the gain in sensitivity [9] in regard to both image quality and quantitative accuracy. Most of the potentially degrading components in 3D mode (normalization, scatter- and attenuation-correction, and calibration) have been addressed within the last several years and show promise of future improvement. However, one factor that is difficult to improve is the intrinsic resolution of a given scanner. A recently published comparison [4] of axial slice width for 2D and 3D modes using phantoms indicates a significant degradation in axial resolution in 3D mode.

For modern PET scanners with intrinsic spatial resolution on the order of 5mm, a difference in FWHM of 2mm can have a large effect on the fraction of counts from nearby locations contributed to a given image plane, and subsequently on axial image resolution. As demonstrated in Figure 1, for an axial resolution described by a FWHM=4.0 mm, 15% of the events recorded within a given plane originate from outside of the plane boundaries. Increasing the FWHM by 2mm results in 35% of the events being misplaced.

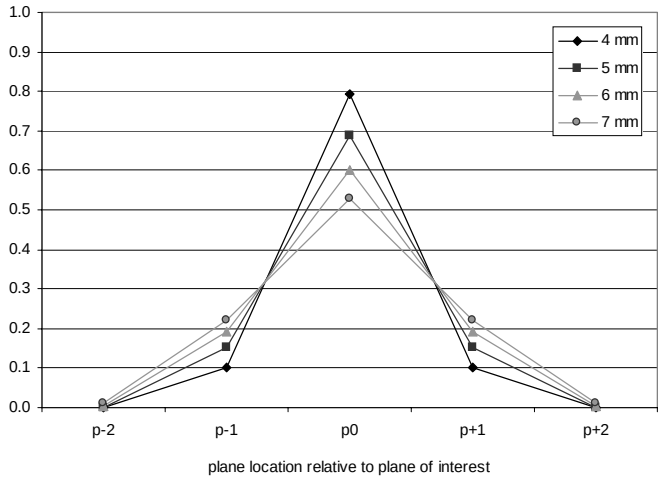


Figure 1: Calculated fraction of events originating from a given plane and assigned to the current plane of interest, for FWHM resolutions of 4, 5, 6, and 7 mm, and a plane width of 4.25mm. Values are based on ratios of integrals of Gaussian distributions.

Much of the literature on 2D/3D differences deals with phantom studies [4-6,9-12] or a different tracer [7,8, 16-18] than FDG. We were interested in examining human subject data to gain insight into what differences, if any, we could anticipate by switching our protocols from 2D to 3D mode, as well as to evaluate the conglomerate effect of all of the corrections with realistic data. We also were attempting to address concerns from some of our researchers that the 3D data are visually and in some respects quantitatively different than 2D data. In particular, 3D images have lower contrast (hotspots in 2D images tend to have higher values than corresponding 3D hot-spots while cool-spots in 2D images tend to be lower), and in general the 3D data appear smoother.

Comparison of 2D and 3D human subject data is complicated since the actual distribution and concentration of radioactivity are not known, and since the accuracy of object-dependent corrections may decrease as the axial and radial symmetry of the object decreases. The current work compares a carefully matched set of 2D/3D cerebral FDG scans in normal humans. One of the major differences that became

evident was the axial resolution, so the possible effects of smoothing due to a difference in the reconstructed axial resolution between 2D and 3D mode for human subjects was examined. We then examined the reliability of ROI analysis typically performed on cerebral FDG PET images for 2D and 3D modes, with particular reference to the effect that axial smoothing in 3D mode might have on the choice of modality.

## II. METHODS

### *A. Human Subject PET Data*

Six (6) subjects were scanned on two occasions as part of an independent study [22], in 2D and 3D mode each time. The second occasion was 4-6 weeks after the first. For the current work, each 2D/3D image pair was considered to be independent. A 30 minute 2D scan was acquired starting 50 minutes after injection of 296 MBq (8 mCi), followed by a 10 minute transmission scan, followed by a 10 minute 3D scan. The emission count-rate fraction was 5% or less of the total count-rate of the T+E transmission measurement. Twice the total number of coincidence events were collected in 3D mode (100M) compared to 2D mode (40-50M); after scatter correction the total number of counts used for reconstruction was similar. Data were corrected with vendor-supplied software (normalization, attenuation, scatter [23], calibration) and reconstructed with filtered backprojection (FBP) using Hanning filters (2D:4.0mm, 3D radial:4.0mm, 3D axial: 8.5mm) with the vendor-recommended parameters at the time of acquisition. Arterialized venous samples were collected, and the resulting measured input functions were used to calculate parametric images of $rCMR_{glu}$ using a variation [24] of the Sokoloff [25] method.

The FDG image data were not spatially normalized to a common reference frame in this work, since we specifically wanted to avoid additional smoothing effects. An in-house manual image alignment program (SPAMALIZE) was used to check for motion in 3 dimensions between each 2D/3D pair. The smallest detectable motion is approximately half of a pixel in any dimension, corresponding to 0.891, 0.891, 2.12 mm for x, y, z, respectively. No motion could be detected.

Comparisons were made of each 2D/3D pair using the following metrics: visual comparison; image subtraction; histogram comparison; and a regression analysis for 20 consecutive subsets of image values with each subset containing a similar number of pixels.

### *B. Axial Smoothing Filter*

Previously published work [3,4] and our own initial observations led us to focus on the difference in axial resolution between 2D and 3D mode as a possible explanation for differences in image quality. By modeling the axial resolution difference, we hoped to estimate the contribution to differences in image quality due to intrinsic axial smoothing in 3D mode. The magnitude of this contribution will limit the extent to which improvements in subsequent processing steps (such as more accurate scatter-correction and reconstruction algorithms) will benefit the image data.

In order to estimate the contribution of axial smoothing in 3D mode relative to 2D, a smoothing filter was created to degrade the 2D images according to the differences in axial resolution. There is a class of axial filters such as proposed by Yang et al. [26] aimed at improving image quality, but these are not well-suited to degrading images in a controlled manner. Pajevic et al. [3] constructed an axial filter by estimating a multiplicative value that would maximize the fit between 2D and 3D measured axial profiles throughout the image volume. This method, while elegant, requires a large set of measurements; similar measurements have been previously published by others [1-2] in summary form, so a location dependent axial smoothing filter was developed to take advantage of these existent works.

Values were culled from published sources on the axial resolution of the GE/Advance in 2D mode [1] and 3D mode [2]. A transaxial smoothing filter was not calculated, since this could make interpretation of results more difficult, and since the 2D/3D transaxial resolutions differ by ~1mm or less. For radii from 0-20 cm, and for each image plane, the axial resolution was determined using published values, interpolating linearly between values where necessary.

A Gaussian distribution was assumed for the axial response function [4, 30]; the validity of this assumption for the present work was demonstrated by measuring the axial response function of a point-source in 2D and 3D mode at a location representative of the cerebral cortex within the PET scanner. Approximately 20 μCi of $[^{18}F]$-$F^-$(aq) was placed in a thick-walled 1/16" I.D. teflon tube, positioned with the tube parallel to the reconstructed image planes. The radioactive droplet was located 4.5 cm radially from the center of the FOV, 4.8 cm below the horizontal laser light (which approximately intersects the center of the FOV), and was moved in 1.5 mm increments every 90 seconds over 43.5 mm for a total of 29 measurements. The scans were centered in image plane 13 (of 35). This process was performed once for 2D mode and repeated for 3D mode. The data were decay-corrected and reconstructed similarly to the human subject data, except no attenuation- or scatter-correction was performed. A circular ROI with 18 pixels ($53.2^2$mm) was placed over the center of the point source in the reconstructed images and the average concentration was extracted from each of the 29 locations for both 2D and 3D. The average ROI values were plotted as a function of distance from plane 13 (of 35) after normalizing the values to yield a unit area under the curve.

The fraction of a Gaussian distribution in an image plane was calculated for the current plane of interest (p0) and the nearest 4 planes (p-2, p-1, p+1, p+2), for Gaussian distributions centered on p0 with FWHM for 2D and 3D modes at each voxel in an image volume. The fractions are named as $F2D_i$ and $F3D_i$, where "i" is the number of planes from the current plane. Weighting factors for nearby pixels were calculated as:

$$w_i = F3D_i * (1 - F2D_i), \quad (1)$$

which yields the fraction of the 3D contribution from a given plane not already accounted for by the 2D contribution. To apply the smoothing filter to the 2D images, each pixel was

assigned the weighted average of itself and the corresponding pixels from the neighboring +/-2 planes:

$$C(x,y,p) = C_p = \sum_{i=p-2}^{p+2} w_i C_I \qquad (2)$$

If the Gaussian distribution extended beyond p+/-2, the remainder was evenly shared with p+/-1, p+/-2. For the largest FWHM used in this filter (<8.0 mm) the remainder beyond p+/-2 (10.6mm) was negligible. In planes near the end of the FOV, weights for planes which would be outside the axial FOV were evenly shared by p0 and p-1 or p+1, if applicable. Data from end-planes did not contribute to this work due to the centered location of the brains and phantoms. Weighting factors for p-2, p-1, p0, p+1, p+2 were then multiplied by the values of the single pixel from each corresponding plane with the same x,y location as the current pixel of interest.

### *C. ROI Analysis Comparison*

Analysis of the human subject data alone cannot discern whether 2D or 3D mode yields values that are more accurate, since the true values are unknown. A series of phantom studies was performed to determine which mode is more accurate for a typical cerebral FDG ROI analysis, and to relate our findings on axial smoothing to known values in a controlled phantom environment. Since many more acquired counts are incorporated into a 3D image, we were particularly interested in whether this provided an advantage for a typical ROI analysis. Similarly, we wanted to determine if there was a threshold of acquired counts below which 3D mode was advantageous.

A phantom with cool and hot spheres of various sizes in a warm background was scanned in 2D and 3D mode. The phantom's radioactive concentration (0.5 to 0.8 μCi/ml) and volume (2750 ml) were designed to simulate a [$^{18}$F]-FDG PET scan of a human head. The phantom was a slightly tapered cylinder (15.0 cm diameter in the center, 15.5 cm height) resting on one of its flat sides. This orientation was selected to reduce the possibility of overlapping artifacts from normalization (scanner dependent) and scatter (object dependent). The phantom contained 4 pairs of hollow plastic spheres (22, 17, 9, 4.7 mm ID) mounted on nylon thread 2cm from the midline; one sphere in each pair was injected with a nominal concentration of half of the warm background (cool-spots), and the other sphere in the pair contained twice the warm background (hot-spots). Four additional pairs of spheres (all 17 mm ID) were positioned lateral to the variously sized spheres. The two smallest "spheres" were in fact plastic cylinders with plugs in both ends, aligned so that the long axis of the cylinders were approximately vertical. The wall thickness of all of the plastic spheroids was 1.5 to 2.0 mm.

Four scans of the phantom were acquired in 2D-HR (High-Resolution) mode, which uses fewer cross-planes per reconstructed plane than the alternate HS or High-Sensitivity mode. The 2D acquisition parameters were: (30, 15, 5, 1 min, with total counts 220M, 95M, 30M, and 5.8M, respectively), followed by four scans in 3D mode (30, 15, 5, 1 min, with total counts 1101M, 477M, 149M, and 29M, respectively), followed by a 20 minute transmission scan. The frame durations were selected to provide acquired counts ranging from the longest duration generally measured for a cerebral FDG scan (30 min) to a much smaller number of counts than is generally acquired (1 min). The concentration for each 3D frame was 68% of the corresponding 2D frame while the total counts obtained for each 3D time frame was a factor of 5 greater than in 2D, yielding a gain in sensitivity similar to that observed by others [9, 20, 21] after scatter-correction.

The standard software from the manufacturer was used for the normalization, scatter correction, attenuation correction (with a radioactive source present in the FOV), and reconstruction (2D: FBP, 30cm FOV, 128x128 pixels, 4.6 mm Hanning filter; 3D: Kinahan-Rogers FBP [27], 30 cm FOV, 128x128 pixels, radial 4.6mm Hanning filter, axial 8.5 mm Hanning filter). The manufacturer currently recommends a 3D axial ramp filter, but a Hanning filter was used so the phantom data would be consistent with the human subject data.

ROIs were placed on each pair of hot and cool spheres to evaluate the reliability of a typical ROI analysis. A series of planar ROIs were placed on subsequent image planes to yield a Volume-of-Interest (VOI) for each sphere. The VOIs were centered on the spheroids and the VOI boundary was well within the actual spheroid boundary to reduce partial-volume effects [28]. The 5 pairs of 17 mm spheroids, as well as 280 warm background VOIs, were used to estimate VOI reliability for 2D and 3D modes; each VOI was centered on a spheroid or background and contained 20 voxels (2.34x2.34x4.25mm) with a total volume of 0.465 cm$^3$, compared to the true volume of a 17 mm sphere of 2.57 cm$^3$. The standard deviation of the VOI averages was used as a comparison metric.

## III. Results and Discussion

### *A. Visual Comparison of Human 2D/3D Pairs*

For all 12 of the 2D/3D pairs, the detectable motion was less than half of a pixel width in any dimension (0.891, 0.891, 2.12 mm for x, y, z, respectively). An automated image registration package (AIR, [29]) was also used to try to quantitate the amount of movement. However, we found that AIR tended to shift the 3D images in a superior direction by approximately 2 mm (unpublished data), which upon close inspection was attributed not to motion but rather to the somewhat larger brain area in 3D mode near the top of the head (see Section II.B), which we attribute in large part to axial smoothing.

The 3D images appear markedly smoother (see Figure 2), even though there is a similar number of total counts in each of the corrected sinogram sets. The difference in average metabolic rate between the individual 2D and 3D pairs ranges from 0.0% to 4%, so the total concentration is conserved between the two modes. This holds true if all pixels are included in the average, or if background pixels (below 0.1mg/min/100g) are excluded. Another difference evident in Figure 2 is the darker hot-spots and whiter cold-spots in the 2D data (e.g. in the striatum and white matter, respectively) which corresponds to differences of 10-20% in hot and cold regions between these quantitative data sets.

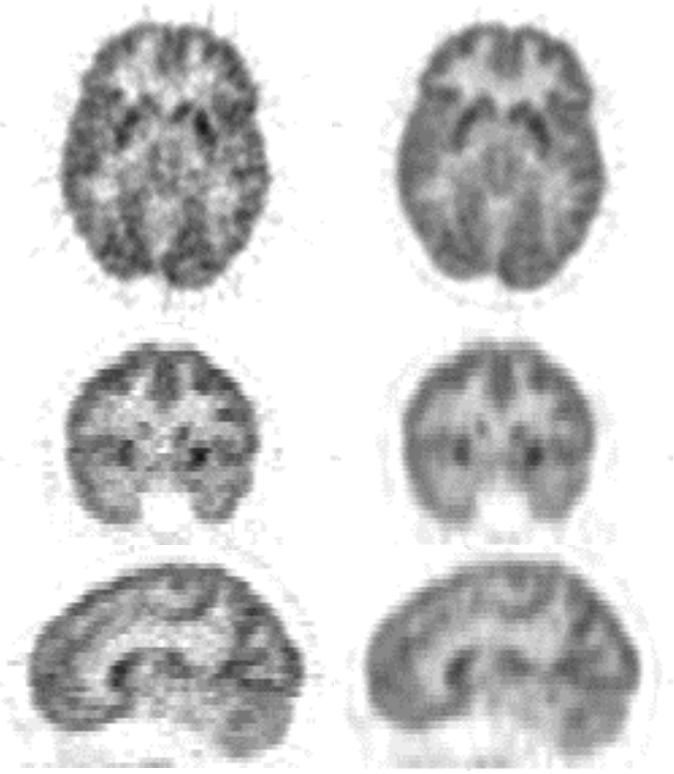


Figure 2: Axial (top), coronal (center) and sagittal (bottom) pairs of 2D (left) / 3D (right) reconstructed images from a representative cerebral FDG PET scan. The same color table was used for the 2D and 3D images so a given gray-level corresponds to the same value of $rCMR_{glu}$ (mg/min/100g) in both image sets.

## *B. Human 2D/3D Image Subtraction*

The pattern of 2D-3D differences is not uniform, but rather the 2D images tend to have greater values in the cortical region near the edge of the brain and in other gray-matter structures. In Figure 3a, a halo in the subtraction images is evident near or outside of the edge of the brain. This is more pronounced toward the top of the head, where the shape of the head changes more rapidly from plane to plane. The axial slice near the center of the brain (bottom row) shows a very small halo, whereas the more superior axial slices show larger halos (middle, top rows). The halo effect is due to a larger region in each 3D image exhibiting values consistent with brain tissue compared to the 2D images. Attempts to explain this halo provoked the axial smoothing filter implemented in this work.

Image subtraction (2D-3D, top row of Figure 3b) shows a pattern of higher values for 2D near the edge of the head within the brain (the dark bands), higher values for 3D near the edge of the head but apparently outside of the brain (the white halo), and slightly lower 2D values toward the center of the brain. These differences may be due to a combination of axial and radial smoothing together with different attenuation- and scatter-correction implementations. Comparison of 2D with 2D axially smoothed images (bottom row of Figure 3b) shows a similar pattern and emphasizes the differences near the edge of the brain, indicating that axial smoothing can account for some of the 2D/3D differences.

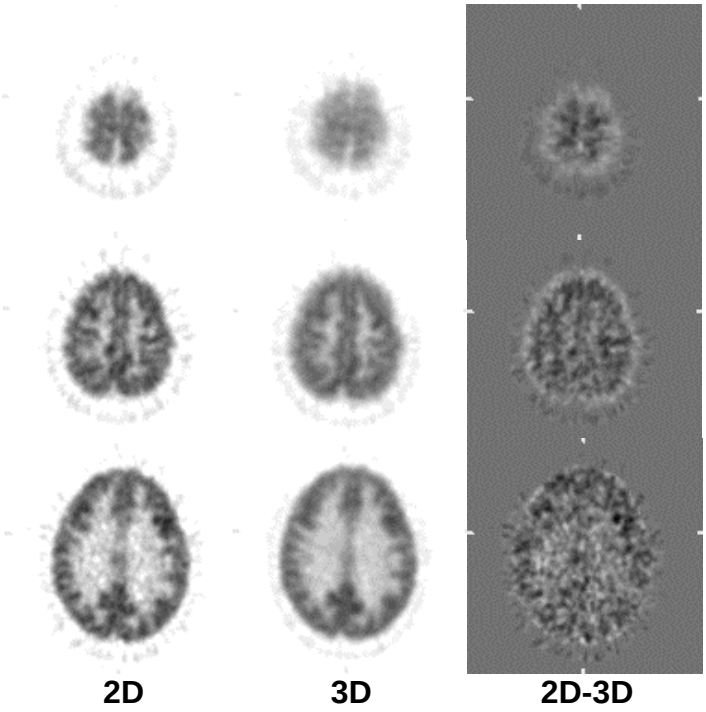


Figure 3a: Image subtraction results (right) for 3D (mid) subtracted from 2D (left), for axial planes 21 (bottom), 27 (center), and 31 (top) of 35. Darker shades indicate where the 2D values are greater than 3D values, lighter shades indicate where 3D values are greater than 2D, and the gray background shade indicates no difference.

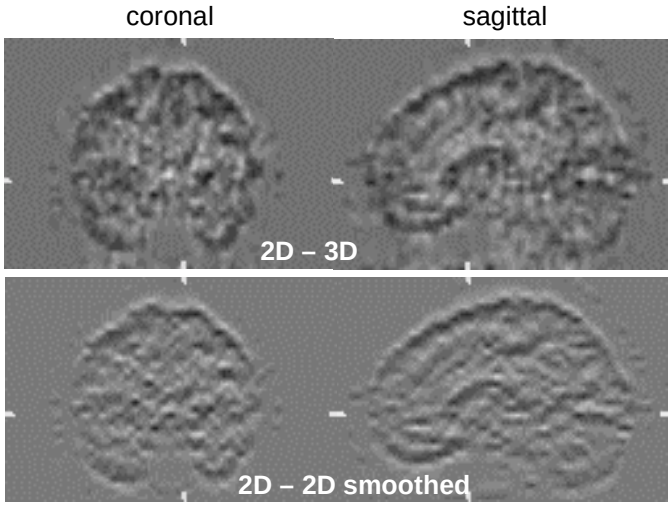


Figure 3b: Image subtraction results for 3D subtracted from 2D (top) and axially smoothed 2D subtracted from 2D (bottom), for the same coronal (left) and sagittal (right) planes shown in Figure 2. The same gray-scale scheme is used as in the subtraction images in Figure 3a. The white hash marks indicate the locations of the orthogonal planes.

## *C. Gaussian Axial Profile Validity*

We found that the assumption of a Gaussian shape for the axial profile was valid for the purposes of constructing an axial smoothing filter, as demonstrated in Figure 4. The peak of the 3D data is shifted approximately half of a measurement increment (0.75 mm) relative to the 2D data, possibly due to

hysteresis in positioning the bed which held the point-source. Both the 2D and 3D profiles agree with a Gaussian fit for the corresponding FWHM to approximately the level of the FWTM, below which the measured profiles are somewhat higher. This is similar to data presented by Pajevic et al. [3], and also to the main findings of Daube-Witherspoon et al. [4], who presented a detailed examination showing that axial response functions in 3D mode (septa out) could be well fit to Gaussian functions, whereas the tails of the distribution with the septa in were somewhat larger than would be predicted from the FWHM. The data shown in Figure 4 are similar except the 3D tails are slightly higher for large distances.

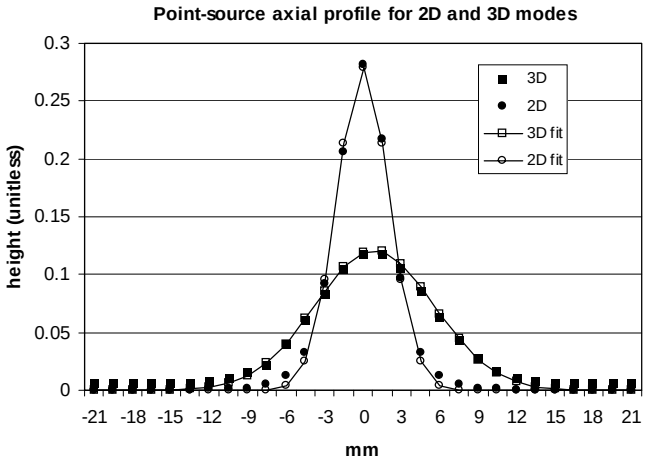


Figure 4: Measured axial profiles for a point-source in 3D (filled squares) and 2D (filled circles) modes. The open squares and circles show the Gaussian distribution fit to the FWHM for the measured 3D and 2D axial profiles, respectively, which are connected by lines. Both measured distributions are scaled to a unit area.

Our axial filter depends on the difference between the 2D and 3D axial profile out to a distance of +/-10.75 mm from the center of a given image plane; differences between the measured and fit data are minimal to at least this distance. Interestingly, the largest difference for 3D mode between the measured data and the Gaussian fit is in the tails, where there is a nearly constant background level of activity. This is most likely due to scattered photons (e.g. off of the gantry), and thus the tails actually represent a scatter-correction problem and are not directly related to the intrinsic axial resolution.

The validity of a Gaussian profile as an approximation of the axial response function justifies the use of previously published values of axial resolution [1,2] to construct our axial smoothing filter, which in turn demonstrates a novel use of this laboriously gathered data.

The accuracy of replicating axial smoothing is limited by the similarities of the reconstruction processes for the axial resolution data and the 2D/3D data of interest. The axial resolution values for 3D mode [2] were reconstructed using an axial ramp filter (8.5 mm), whereas our human-subject and phantom data employed an axial Hanning filter (8.5 mm). Thus, our axial filter underestimates the amount of axial smoothing needed for the 2D to simulate the 3D data.

## *D. Histogram Analysis*

Pixels with a background value greater than 0.1 mg/min/100g in either element of a 2D/3D pair were used to create histograms for each 2D and 3D image volume. As shown in Figure 5, the pixels with the largest values in the 2D images have smaller values in the 3D data, while the pixels with smaller values (from ~2.0 to 7.0 in Figure 5) in 2D mode have correspondingly larger values in 3D mode. Generally, the most active regions in the 2D images become relatively less active in the 3D data. This can cause a significant difference for analysis such as ROI placement on hot-spots or searching for areas of maximal activation, as the most active regions are the pixels that differ most between 2D and 3D.

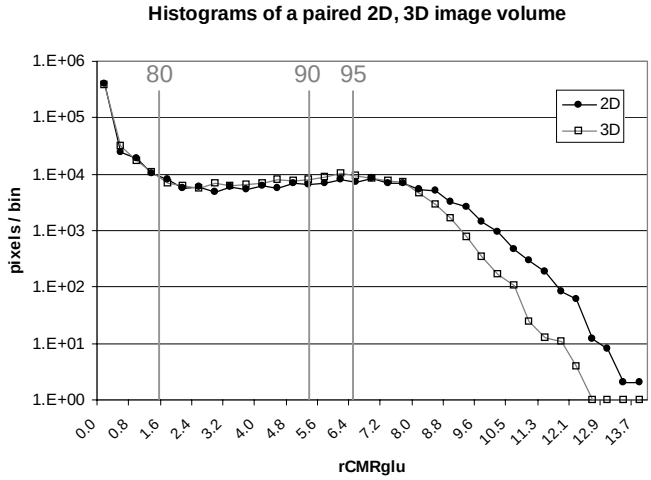


Figure 5: A histogram of all reconstructed image values from the entire image volume of a single representative subject. The vertical gray lines indicate the thresholds for percentiles of 80, 90, and 95. Note the log-based ordinate, which compresses differences between the two modes for the lower values (< 2.0).

## *E. Regression Analysis*

A regression analysis was performed to estimate the fraction of the difference between 2D and 3D modes that could be attributed to the larger inherent axial smoothing of 3D mode. Each 3D value was plotted as a function of the corresponding 2D pixel (see Figures 6), and the values from each scan pair were placed into 20 bins, with approximately the same number of values in each bin. The division between each bin is perpendicular to the line of identity. Instead of finding the slope and intercept for a group of points, the Center-of-Mass (CoM) of each bin was calculated. A plot of the regression line for each bin (not shown) would overlay the corresponding CoM, and would be tangent to the line connecting the CoM points. The distance ($d_{CoM}$) from each CoM point to the line of identity is a measure of the mismatch between the two data sets in that bin. The CoM is above the line of identity where the 3D pixel values are higher than their corresponding 2D values, and below the line of identity where 3D values are less than corresponding 2D values. After the 2D axial smoothing filter is applied, the CoM is closer to the line of identity (see

Figure 6b) for most bins, and the variance between the two data sets is reduced.

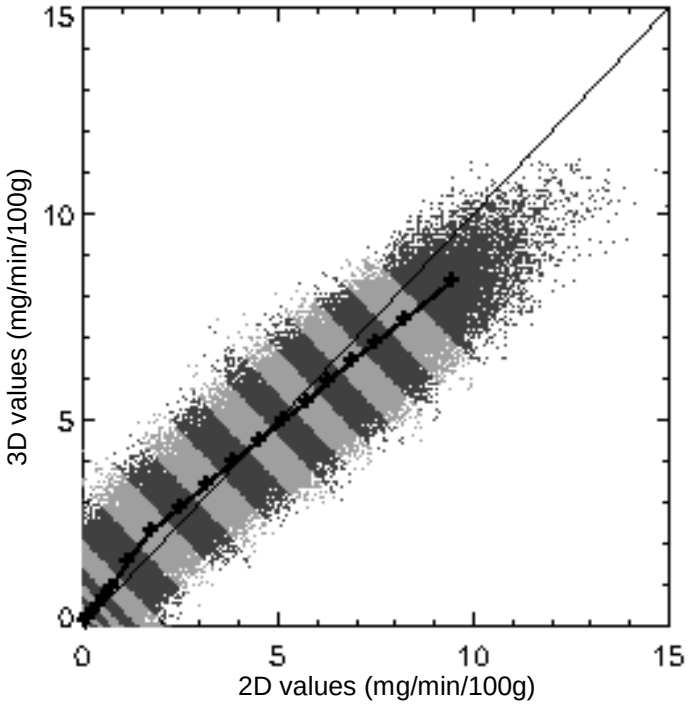


Figure 6a: Scatter plot of 3D vs. 2D pixel values for a single subject. The diagonal line of identity shows 3D=2D. Each bin is represented by an alternating gray-level in the scatter-plot. The location of the Center-of-Mass (CoM) of each bin is indicated by a (+).

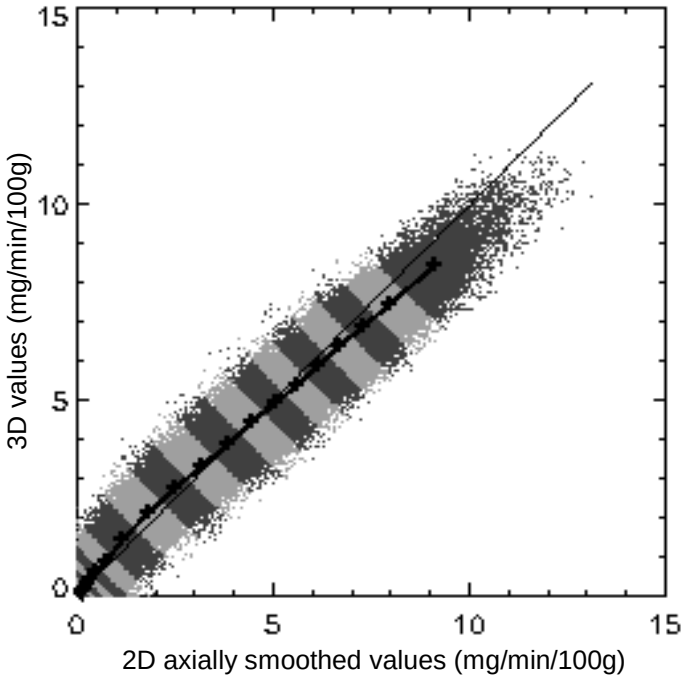


Figure 6b: Scatter plot of 3D vs. axially smoothed 2D pixel values for the same subject as shown in Figure 6a.

The average of each CoM in each bin was calculated for all 12 scan pairs, for 2D:3D and axially-smoothed-2D:3D (see Figure 7a). In all bins except the first, the absolute value of the CoM in the axially smoothed pair is smaller, indicating a better match with the 3D data. More interesting is the pattern of the 2D:3D plot. Positive values indicate bins where the 3D data tend to be higher than the 2D data, and negative values show where the 3D data are lower. Areas of higher concentration (hot-spots) in the 3D data have reduced values compared to the 2D data, while cold-spots have increased values. These results are similar to the histogram results shown in Figure 5, but here each 2D pixel has been paired with its corresponding 3D pixel for a more specific comparison. This discrepancy can have an important effect on certain types of image analysis, such as calculating the ratio of a value from a region of specific uptake to another region with no specific uptake.

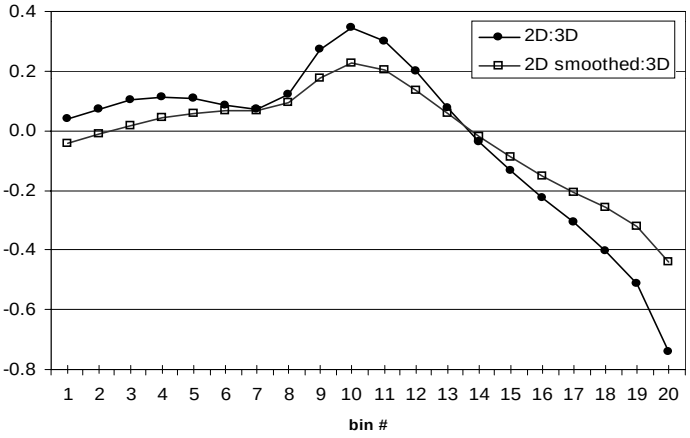


Figure 7a: Distance from bin Center-of-Mass (CoM) from line of identity, averaged over 12 scan pairs for each bin.

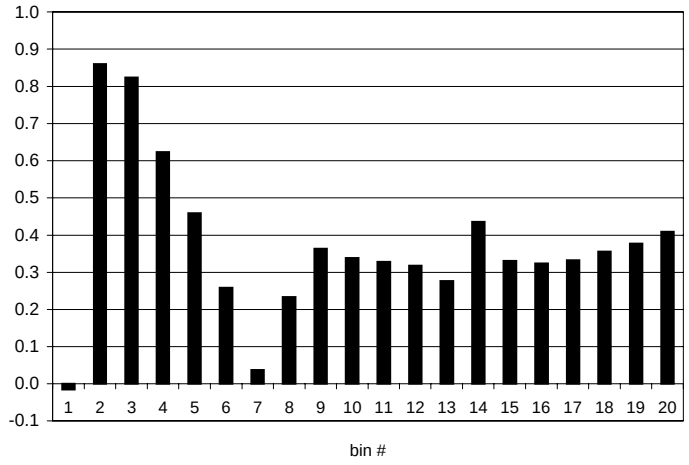


Figure 7b: Fraction of difference between 2D, 3D scans attributed to 3D axial smoothing (calculated as in Eq. 3), for 20 distinct data ranges (bins) averaged over all 12 scan pairs.

The fraction of the difference between images acquired in 2D and 3D mode that can be explained by the axial smoothing filter is shown for each bin in Figure 7b, calculated as:

$$f = 1 - \left( \frac{d_{CoM}(\text{2D smoothed})}{d_{CoM}(\text{2D})} \right) \qquad (3)$$

Differences between 2D and 3D modes due to 3D axial smoothing are fairly similar throughout the bins having medium to higher levels of concentration, and can account for 30% to 40% of the observed differences between these two modes. However, it is important to note that these differences are neither linear nor monotonically changing with respect to the image values, which impinges on the accuracy of subsequent data analysis. For example, the higher fractional differences in Figure 7b for lower values (bins 2-4) can be partly attributed to the fact that many of the pixels with lower values are located near the edge of the brain and are thus more susceptible to axial smoothing.

## *F. Recovery Coefficients*

Recovery coefficients were estimated for hot and cool spheres relative to a warm background (Figure 8). The results for the hot spheres are similar to those obtained previously [2] for a broader range of diameters. The ROIs for the smallest spheres only contain 6-8 pixels, so the values are not as statistically reliable as the larger ROIs. These data are presented not to replicate earlier work [2], but rather to demonstrate that 2D mode is more accurate than 3D mode for the range of sphere sizes and activity concentration examined in the current work, and to confirm our observations that cool spots in our human-subject FDG scans generally have larger values for 3D mode than for 2D mode.

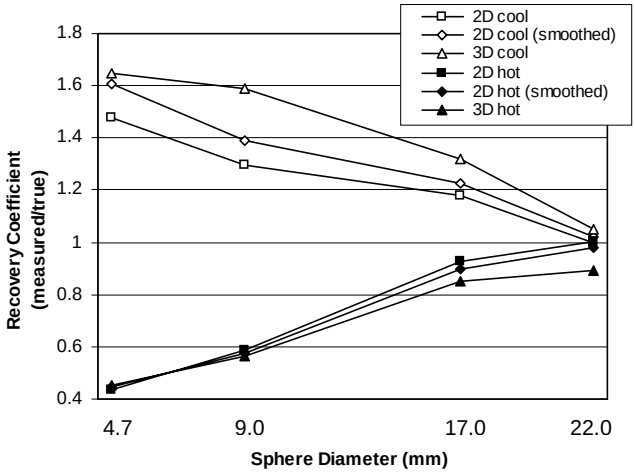


Figure 8: Recovery coefficients for spheroid objects with nominal inner diameters of 4.7, 9.0, 17.0, and 22.0 mm, for the 30 minute time frame.

The 3D cool spots consistently recovered less of the actual concentration than did the corresponding 2D cool spots, whereas the 3D hot spots are closer to their 2D counterparts. This may be explained in part by the long tails evident in Figure 4, in that for 3D mode there is not only more axial smoothing but also a much larger scatter fraction.

## *G. ROI Reliability*

Somewhat surprisingly, the increased number of acquired counts in 3D mode does not yield a significant increase in ROI reliability for a typical FDG scan. The reliability of average ROI values for 5 similar ROIs was estimated for 4 different time frames corresponding to a broad range of acquired counts, using the standard deviation of the individual values within each frame as a metric (see Figure 9a).

These are plotted as a function of frame duration rather than total acquired counts to emphasize that for the concentration range typical of most human cerebral FDG protocols, there is little difference between 2D and 3D modes for typical frame durations (10 – 30 minutes). The standard deviation is similar for both modes except for the shortest frame (1 minute) where 3D mode shows an advantage.

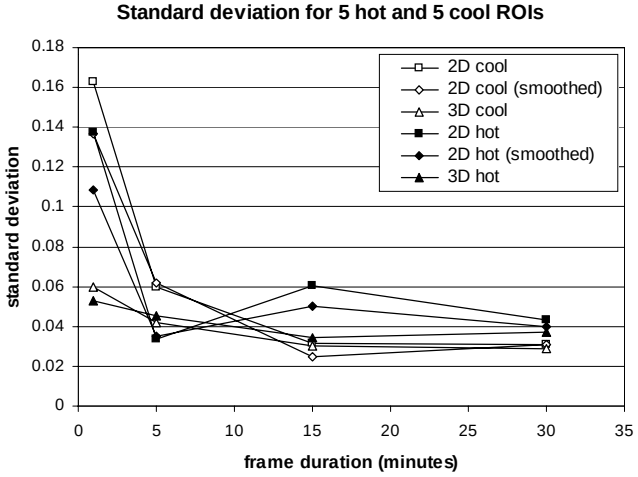


Figure 9a: Standard deviation of ROI values from 5 cool and 5 hot 17mm spheres for 4 time frames (1, 5, 15, 30 minutes). The frame durations correspond to a range of total counts in 2D from 5.9M to 220M, and in 3D from 29M to 1101M.

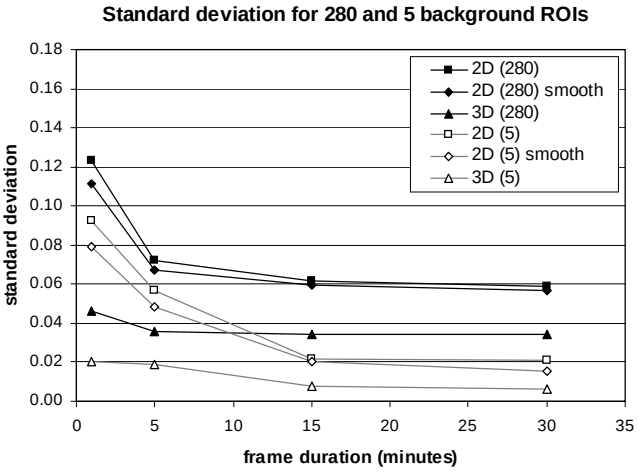


Figure 9b: Standard deviations of 280 ROI values from the warm background, with a subset of the standard deviation from 5 randomly selected ROIs. The ROIs were the same size as those used for the 17mm ROIs in Figure 9a.

The standard deviations for 280 of the 17mm-sized background ROI average values are shown in Figure 9b, along with standard deviations from a representative subset of five background ROIs. The pattern is similar to that shown in Figure 9a for the limited number (five) of hot- and cool-spot ROIs, in that the 2D data show a marked increase in the standard deviation for the 1-minute frame.

In contrast to the hot- and cool-spot data, the 3D data for the background ROIs show a lower standard deviation for all frames. The standard deviations for the 2D and axially-smoothed 2D sets are quite similar, indicating that axial smoothing alone cannot account for the increased reliability of the 3D data. This difference is probably due to at least three factors: (i) the small number of ROIs in the hot- and cool-spot data and consequent sensitivity to individual values; (ii) the increased covariance in 3D due to the reconstruction and correction algorithms as well as to axial smoothing; and (iii) the larger number of acquired counts in 3D mode and consequent improvement in Signal:Noise ratio.

It is difficult to measure the standard deviation of a group of hot-spots; if there are enough hot-spots to yield statistically reliable results, the hot-spots then merely constitute a new warmer background. The background ROI results are statistically more reliable than the hot- and cool-spot data due to the larger number of ROIs (280 vs. 5). However, it is not clear that the lower standard deviation for 3D ROIs in the background necessarily holds true for the hot- and cool-spots, since in 3D mode the values of hot- and cool-spots are lower and higher, respectively, compared to values near the global average (see Fig. 6a).

## IV. Conclusions

For the human FDG protocol investigated in this work, there were approximately the same number of events contributing to the reconstructed images after correcting the data for scatter. However, this similarity is not reflected in the images, as the 3D data are significantly smoother. Approximately 30-40% of this difference can be explained by increased axial smoothing in 3D mode. This may be a conservatively low estimate due to the different axial reconstruction filters used in the axial resolution data [2] and our human-subject data. The relative contribution of the various corrections (normalization, scatter, and attenuation) and the reconstruction algorithm to the 2D/3D differences was not determined. Further investigation is required to distinguish between the intrinsic differences in 2D and 3D modes due to the removal of collimating septa, as opposed to the limitations of the algorithms used to correct and reconstruct the data.

Slightly greater quantitative accuracy was obtained in 2D mode, based on the ROI recovery coefficients shown here. However, other work [2] indicates these results may not be generally applicable to larger uniform regions; furthermore, these results may not apply to scanning protocols with a much larger or smaller radioactivity concentration. Differences between 2D and 3D modes were not constant for all values; rather, they were greatest for large and small values within an image, which can adversely affect particular types of image analysis (such as ratios of hot-spots to cooler reference regions) and can also make comparison of 2D and 3D results problematic.

The much larger number of detected coincidence events obtained with 3D mode (5 to 8 times higher) had little effect on the reliability of ROI values obtained for the 17mm ROIs corresponding to a typical FDG protocol, with a range of total acquired counts of 2D:20-50M, 3D:100-300M. The advantage of using 3D mode only became apparent for a relatively low number of detected coincidence events (2D:6M, 3D:29M, for the first frame shown in Figure 9a). In cases where there is such a low number of events, due either to limited tracer concentration or limited counting duration, 3D mode may be advantageous.

An increased reliability for 3D mode was found for the warm background ROIs across all time frames (Figure 9b). These values are least likely to be affected by loss of contrast in 3D mode, and it is unclear to what extent these results are applicable to warm- and cool-spots. This aspect particularly bears further investigation for individual protocols.

Much of the published literature examining 2D/3D differences has found that 3D mode offers distinct advantages; the findings in this work failed to support this. However, most of the extant 2D/3D comparison literature deals with relatively count-poor scan protocols such as bloodflow with [$^{15}$O]-$H_2O$ [17] or neurotransmitter studies [7, 8], which benefit from the increased counts obtained in 3D mode. Conversely, a recent comparison of 2D/3D PET in a whole-body application [5] found no significant difference in lesion detectability between the two modes. Compared to many types of PET studies, FDG scans are relatively count-rich due to favorable tracer uptake, long halflife, and long scan times. The current work indicates that if a cerebral FDG PET scan is not limited by acquired counts, no particular benefit is gained from 3D mode.

For the FDG protocol investigated here, 2D mode is preferable due to its increased quantitative accuracy with little loss in reliability.

## V. Acknowledgements:

This work was supported by the DHHS under NIH grant R01 MH40747-12.

## VI. Bibliographic References:

[1] DeGrado TR, Turkington TG, Williams JJ, Stearns CW, Hoffman JM, Coleman RE, “Performance characteristics of a whole-body PET scanner”, *J. Nucl. Med.*, 35:1398-1406, 1994.

[2] Lewellen T, Kohlmyer S, Miyaoka R, Schubert S, Stearns C, “Investigation of the count rate performance of the General Electric ADVANCE positron emission tomograph”, *IEEE Trans. Nucl. Sci.*, 42:1051-1057, 1995.

[3] Pajevic S, Daube-Witherspoon ME, Bacharach SL, Carson RE, “Noise characteristics of 3-D and 2-D PET images”, *IEEE Trans. Med. Imag.*, 17(1):9-23, 1998.

[4] Daube-Witherspoon ME and Carson RE, “Axial slice width in 3D PET: characterization and potential improvement with axial interleaving”, *Phys. Med. Biol.*, 43(4):921-8, 1998.

[5] Raylman RR, Kison PV, Wahl RL, “Capabilities of two- and three-dimensional FDG-PET for detecting small lesions and lymph nodes in the upper torso: a dynamic phantom study”, *European J. Nuc. Med*., 26(1):39-45, 1999.

[6] Sossi V, Oakes TR, Ruth TJ, "A phantom study evaluating the quantitative aspect of 3D PET imaging of the brain", *Phys.Med.Biol.*, 43(9):2615-2630, 1998.

[7] Sossi V, Oakes TR, Chan G, Schulzer M, Ruth TJ, "Quantitative comparison of three- and two-dimensional PET with human brain studies", *J.Nucl.Med.*, 39(10):1714-9, 1998.

[8] Trebossen R, Bendriem B, Ribiero MJ, Fontaine A, Frouin V, Remy P, “Validation of the three-dimensional acquisition mode in positron emission tomography for the quantitation of [18F]fluoro-DOPA uptake in the human striata”, *J. Cereb. Blood Flow Metab.*, 18(9):951-9, 1998.

[9] Li HH, Votaw JR, "Spatial variation of SNR in 2D & 3D Neuro PET", *Proc. 1995 IEEE NSS/Medical Imaging Conference, Oct. 21-28, San Francisco, USA*, pp. 1079-1083, 1995.

[10] Daube-Witherspoon M, Bacharach S, Carson R, Influence of activity outside the field-of-view on 3-D PET imaging. *J. Nucl. Med*., 36:184P, 1995.

[11] Erlandsson K, Strand S-E, "Improved axial resolution in 2D PET with 3D reconstruction", *Proc. 1995 IEEE NSS/Medical Imaging Conference, Oct. 21-28, San Francisco, USA*, pp. 1267-71, 1995.

[12] Holm S, Toft P, Jensen M, "Estimation of the noise contributions from blank, transmission and emission scans in PET", *IEEE Trans. Nuc. Science*, 43(4), 2285-91, 1996.

[13] Badawi RD, Marsden PK, Cronin BF, Sutcliffe JL, Maisey MN, "Optimisation of noise-equivalent count rates in 3D PET", *Phys. Med. Biol.*, 41:1755-76, 1996.

[14] Badawi RD, “3D-mode acquisition in clinical PET”, *Nuclear Med. Comm.*, 18(9):801-4, 1997.

[15] Li HH, Votaw JR, “Optimization of PET activation studies based on the SNR measured in the 3-D Hoffman brain Phantom”, *IEEE Trans. Nucl. Sci*, 17(4):596-605, 1998.

[16] Morenu-Cantu JJ, Thompsen CJ, Zatorre RJ, “Evaluation of the ECAT EXACT HR+ 3-D PET scanner in H2(15)O brain activation studies: dose fractionation strategies for rCBF and signal enhancing protocols”, *IEEE Trans Nucl. Sci*.,17(6):979-85, 1998.

[17] Isoardi RA, Townsend DW, Carter CS, Herbster A, Dachille MA, Meltzer CC, “A study of the injected dose for brain mapping on the ECAT HR+: activation images for a parametric verbal working memory task”, *Neuroimage*, 9(1):145-53, 1999.

[18] Chmielowska J, Coghill RC, Carson R, Ishii K, Chen R, Hallet M, Herscovitch P, “Comparison of PET [O15]water studies with 6-minute and 10-minute interscan intervals: single-subject and group analysis”, *J. Cereb. Blood Flow Metab.*,19(5):47-59, 1999.

[19] Spinks TJ, Miller MP, Bailey DL, Bloomfield PM, Livieratos L, Jones T, “The effect of activity outside the field of view in a 3D-only whole-body positron tomograph”, *Phys. Med. Biol.*, 43:895-904. 1998.

[20] Cherry SR, Dahlbom M, Hoffman EJ, "3D PET using a conventional multi-slice tomograph without septa", *J. Comput. Assist. Tomog*., 15:655-68, 1991.

[21] Spinks TJ, Jones T, Bailey DL, Townsend DW, Grootoonk S, Bloomfield PM, Gilardi M-C, Casey ME, Sipe B, Reed J, "Physical performance of a positron tomograph for brain imaging with retractable septa", *Phys. Med. Biol.*, 37:8, pp.1637-55, 1992.

[22] Hochachka PW, Clark CM, Brown WD, Stone CS, Nickles RJ, Holden JE, “Effects on regional brain metabolism of prolonged high altitude exposure. A study of six U.S. Marines”, *Am. J. Physiol*., 46:R314-319, 1999.

[23] Stearns C, “Scatter correction method for 3D PET using 2D fitted Gaussian functions”, *J. Nucl. Med*., 36:105P, 1995.

[24] Phelps ME, Huang SC, Hoffman EJ, Selin C, Sokoloff L, Kuhl DE, "Tomographic measurement of local cerebral glucose metabolic rate in humans with (F-18)2-fluoro-2-deoxy-D-glucose: Validation of method", *Ann. Neurol.* 6:371-388, 1979.

[25] Sokoloff L, Reivich M, Kennedy C, Des Rosiers MH, Patlak CS, Pettigrew KD, Sakurada O, Shinohara M, "The [14C]deoxyglucose method for the measurement of local cerebral glucose utilization: Theory, procedure, and normal values in the conscious and anesthetized albino rat", *J. Neurochemistry*, 28:897-916, 1977.

[26] Yang J, Huang SC, Lin KP, Czernin J, Wolfendrin P, Dahlbom M, Hoh CK, Phelps ME, "A new axial smoothing method based on elastic mapping", *Proc. 1995 IEEE NSS/Medical Imaging Conference, Oct. 21-28, San Francisco, USA*, pp. 1420-24, 1995.

[27] Kinahan PE, Rogers JG, “Analytic 3-D image reconstruction using all detected events”, *IEEE Trans. Nucl. Sci*., 36(1):964-968, 1989.

[28] Hoffman EJ, Huang SC, Phelps ME, "Quantitation in positron emission computed tomography: 1. Effect of object size", *J. Comput. Assist. Tomogr*., 3:299-308, 1979.

[29] Woods RP, Grafton ST, Holmes CJ, Cherry SR, Mazziotta JC, "Automated image registration I: General methods and intrasubject, intramodality validation", *J. Comput. Assist. Tomogr*., 22(1):139-152, 1998.

[30] Chen CH Muzic RF, Nelson AD, Adler LP, “Simultaneous recovery of size and radioactivity concentration of small spheroids with PET data”, *J. Nuc. Med*., 40(1):118-30, 1999.